



# Influence of corrugation geometry on the performance of structured packings: an experimental study<sup>☆</sup>

Ž. Olujić<sup>a,\*</sup>, A.F. Seibert<sup>b</sup>, J.R. Fair<sup>b</sup>

<sup>a</sup> *Laboratory for Process Equipment, Delft University of Technology, Leeghwaterstraat 44, 2628 CA Delft, The Netherlands*

<sup>b</sup> *Separations Research Program, University of Texas at Austin, 10100 Burnet Road, Austin, TX 78758, USA*

Received 16 June 1999; received in revised form 4 October 1999; accepted 4 October 1999

## Abstract

While the utilisation of corrugated sheet structured packings is well established, these gas–liquid-contacting devices are still not well understood. A contributing reason is the rather limited publicly available performance data, most of which have been obtained from relatively small columns. A recent comparison of data from the 1.2 m Fractionation Research, Incorporated (FRI) and from the 0.43 m Separations Research Program (SRP) columns show excellent agreement based on equivalent packings. This is significant since the FRI column is considered to be of industrial scale. As a result, we sought to create an expanded data base emphasising packing geometric variations, using packings from a single manufacturer (J. Montz). Hydraulic characteristics of the same packings had been studied previously using air–water simulators at TU Delft. Total reflux distillation experiments were carried out at SRP using a bed height of 3.3 m for all packings. The cyclohexane–*n*-heptane system was utilized because of the availability of comparative data. The operating pressure was varied from 0.33 to 4.14 bar, to determine the effect of physical properties. The resulting data provided insight into the nature and effect of corrugation angle, specific surface area, and surface texture on pressure drop, capacity and efficiency. In this paper we report the results and also discuss the implications of the observations on model development and design. © 2000 Elsevier Science S.A. All rights reserved.

**Keywords:** Structured packing; Corrugated sheets; Total reflux distillation; Mass transfer efficiency; Hydraulic performance

## 1. Introduction

Although the technology associated with the use of structured packings may be considered mature, there is still inadequate experimental evidence in the open literature to provide a firm basis for the development and validation of general and reliable models for predicting packing performance. Most of the published performance data, obtained with corrugated metal sheet packings [1–4] are based on the standard corrugation inclination angle of 45° and a specific surface area in the range 220–250 m<sup>2</sup>/m<sup>3</sup>. Yet most manufacturers offer packings with various surface areas and a corrugation angle of 60°, to satisfy growing application

needs, particularly those for increased capacity. While early designs using the packings were executed with a great deal of confidence, there were notable failures indicating a lack of fundamental understanding of the mechanisms of phase contacting. A recent evaluation of pressure drop models [5], using hydraulic data obtained for different packings, showed that the models do not properly account for the effect of corrugation angle. The conclusion was clear; a systematic study was needed to elucidate the effects of geometry variations, especially corrugation angle.

An opportunity for a such a study came when J. Montz decided to determine the corrugation angle effect with its B1 and BSH series packings, using a conventional pilot scale distillation column available at the Separations Research Program (SRP) of the University of Texas at Austin. The revealing effects of packing geometry and corrugation angle on mass transfer and hydraulic performance are presented and discussed below.

<sup>☆</sup> Based on a paper presented at the 1999 AIChE Spring National Meeting, Houston, 14–18 March 1999.

\* Corresponding author. Tel.: +31-15-2786674; fax: +31-15-2786975.

E-mail address: z.olujic@wbmt.tudelft.nl (Ž. Olujić)

## 2. Experimental setup and procedure

Total reflux tests were carried out with six Montz packings using the cyclohexane–*n*-heptane test mixture. The operating pressure was varied from 0.33 to 4.14 bar to evaluate the effects of physical property changes. These studies allowed the determination of the influence of variations in micro and macro geometry on mass transfer efficiency, pressure drop and capacity. The geometrical characteristics of the packings tested are given in Table 1. A photograph (Fig. 1) shows the elements and surface designs of B1 (embossed sheet metal, non-perforated) and BSH (expanded metal, perforated) packings.

The SRP total reflux distillation system comprises a conventional 0.428 m i.d. well-insulated distillation column, a kettle reboiler heated with 9 bar steam, and a shell-and-tube condenser cooled with chilled (7°C) water. As indicated in Fig. 2, the lower half of the column is typically used for the testing of internals, allowing installation of packed bed heights up to 3.4 m. The major dimensions of the test section are shown separately in Fig. 3. The packing is supported with a flat grid, and the bottom liquid sampler is installed directly under the support plate. The top liquid sample is taken from the reflux return line. Intermediate liquid samplers were not provided in this study, to eliminate

the possibility of maldistribution caused by the samplers. Reflux was returned by gravity onto a collector plate with a centrally placed downcomer pipe feeding the liquid distributor. All tests were carried out using a Montz-type narrow trough distributor with 21 symmetrically arranged drip tubes, corresponding to 145 drip points per m<sup>2</sup> of column cross sectional area. The distance between the drip tubes and the top of the packing was approximately 20 mm in all cases. The packing layers consisted of single elements each rotated by 90° with respect to the adjacent elements.

The pressure drop was measured using two commercially available differential pressure cells, one for the range 0–12.5 mbar, and the other for a range from 0 to 50 mbar, with high and low pressure gauges placed directly below the packing support plate and above the distributor, respectively. Both cells were purged with nitrogen to prevent hydrocarbon condensation. The temperatures were measured in the vapor space above and below the packing.

The structured packing was new and installed carefully to ensure no gaps existed between the elements. The surface of the packing was clean and contained no residual cutting oil. After the installation of the packing and closing of the column, the experimental system was pressure-checked to eliminate any possible leaks. The column was then filled with an initial charge of test

Table 1  
Geometrical features of the J. Montz packings tested

| Packing    | $a_p$ (m <sup>2</sup> /m <sup>3</sup> ) | $\alpha$ (°) | $\epsilon$ (–) | $h_{pw}$ (m) | $h_{corr}$ (m) | $b_{corr}$ (m) | $s_{corr}$ (m) |
|------------|---|--------------|----------------|--------------|----------------|----------------|----------------|
| B1-250     | 244                                     | 45           | 0.98           | 0.197        | 0.0120         | 0.0225         | 0.0165         |
| B1-250.60  | 245                                     | 60           | 0.98           | 0.211        | 0.0120         | 0.0223         | 0.0164         |
| B1-400     | 394                                     | 45           | 0.96           | 0.197        | 0.0074         | 0.0140         | 0.0103         |
| B1-400.60  | 390                                     | 60           | 0.96           | 0.215        | 0.0074         | 0.0143         | 0.0103         |
| BSH-400    | 378                                     | 45           | 0.97           | 0.194        | 0.0074         | 0.0151         | 0.0106         |
| BSH-400.60 | 382                                     | 60           | 0.97           | 0.215        | 0.0074         | 0.0148         | 0.0105         |

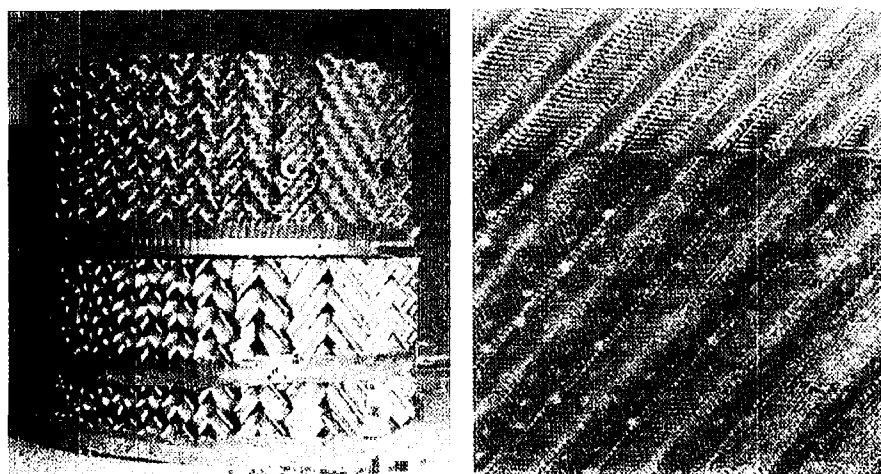


Fig. 1. Packing element, corrugation and surface designs: BSH (expanded metal with holes) and B1 (closed, shallow embossed surface).

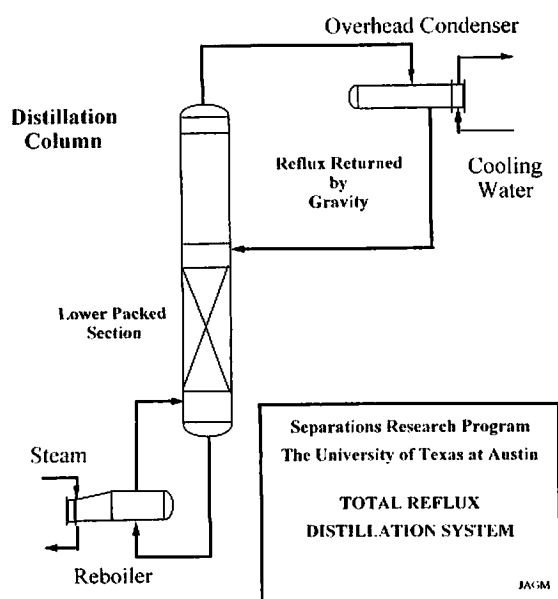


Fig. 2. Schematic of the total reflux distillation system.

mixture, roughly 30 mol% cyclohexane and 70 mol% *n*-heptane. Distillation was initiated by allowing steam to enter the reboiler at approximately 60% of the

estimated flooding rate. After about 1 h the composition was checked and adjusted if necessary. With the system composition set, the flood point was determined by step increases in the heat load until the flooding limit was reached, indicated by a sudden increase in pressure drop that continued to rise during the procedure. A visual observation through the column sight glass was also used to verify the flooding condition.

When the flood point had been determined, the column was operated at predetermined heat loads, and samples at each load were taken for efficiency determination. The first sample was taken 1 h after establishing a measuring point and subsequently samples were taken at 45-min intervals to determine a true steady state condition. Usually the steady state was achieved in 60–90 min after a change in heat load. The samples were analysed by gas chromatography using a TCD detector and each sample was processed at least twice through the chromatograph. Standards for calibration of the chromatograph were prepared gravimetrically. Separate calibrations were made for the bottoms and reflux composition range. An integrator program was used to select the appropriate calibration curve for the composition range.

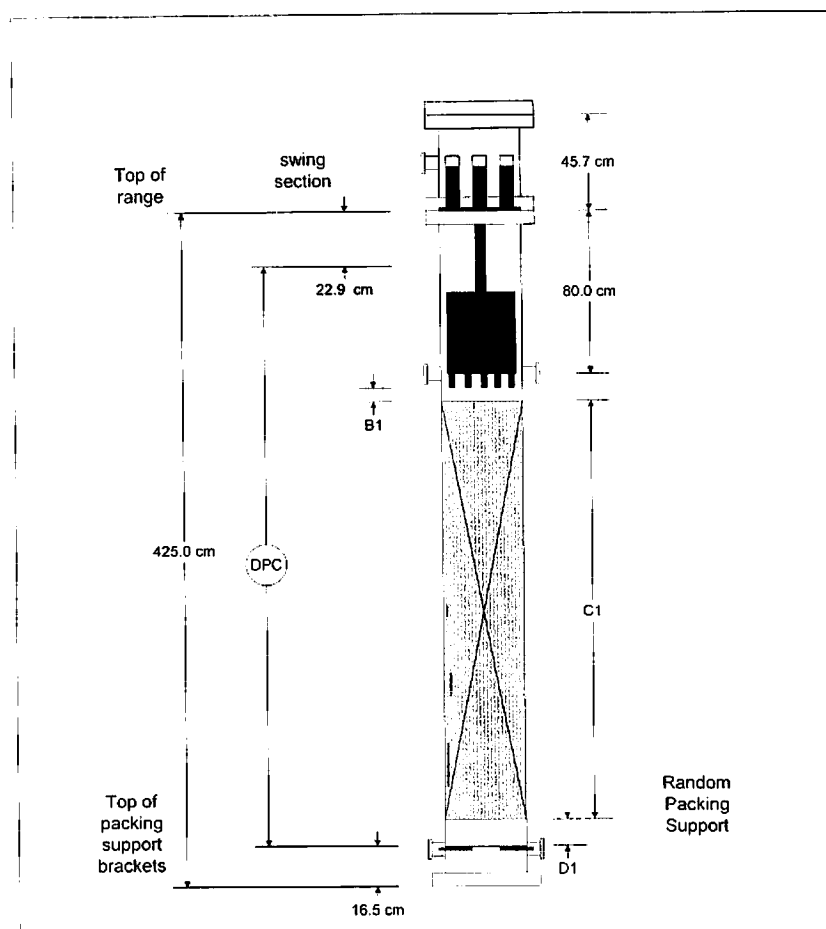


Fig. 3. Schematic dimensions of the packed section used in the J. Montz structured packing tests.

Table 2  
Physical properties of the cyclohexane–*n*-heptane system (average at bottom conditions)

| Physical property   | Pressure (bar) |          |          |          |
|---|----------------|----------|----------|----------|
|   | 0.33           | 1.03     | 1.66     | 4.14     |
| Temperature (°C)  | 61             | 97       | 114      | 154      |
| Liquid density (kg/m <sup>3</sup> )   | 657            | 625      | 609      | 561      |
| Liquid viscosity (Pa s)   | 4.31 E–4       | 2.97 E–4 | 2.31 E–4 | 1.61 E–4 |
| Liquid diffusivity (m <sup>2</sup> /s)  | 2.72 E–9       | 4.44 E–9 | 6.11 E–9 | 9.17 E–9 |
| Vapor density (kg/m <sup>3</sup> )  | 1.19           | 3.53     | 5.45     | 13.14    |
| Vapor viscosity (Pa s)  | 6.94 E–6       | 7.78 E–6 | 8.33 E–6 | 9.17 E–6 |
| Vapor diffusivity (m <sup>2</sup> /s)   | 11.4 E–6       | 4.17 E–6 | 3.06 E–6 | 1.39 E–6 |
| Surface tension (N/m)   | 0.017          | 0.014    | 0.012    | 0.008    |
| Relative volatility (–)   | 1.86           | 1.64     | 1.57     | 1.42     |
| Stripping factor (–)  | 1.5            | 1.35     | 1.32     | 1.21     |
| Schmidt number (–)  | 0.51           | 0.53     | 0.50     | 0.50     |
| Liquid load (m <sup>3</sup> /m <sup>2</sup> per h) at $F_G = 1.5$ m/s (kg/m <sup>3</sup> ) <sup>0.5</sup> | 9              | 16.2     | 20.7     | 34.9     |

In this study, mass transfer efficiency and pressure drop are reported for the total reflux operation. The efficiency is reported in terms of height equivalent to a theoretical plate (HETP), calculated from the ratio of packed height to the number of equilibrium stages of separation. The equilibrium stages were calculated from measured compositions using the Fenske relationship for minimum stages and relative volatilities at the bottom and top compositions. The number of stages so determined were confirmed by stage-to-stage calculations; for both approaches vapour–liquid equilibria were based on the analysis of this system by Lenoir and Sakata [6]. Determination of transfer units for total reflux conditions provides values directly convertible to stages obtained by the Fenske method. The HETP and pressure drop are plotted against the  $F$ -factor (the product of superficial vapour velocity and the square root of the vapour density). The reported  $F$ -factor is based on the bottom bed conditions. Table 2 shows the physical properties.

### 3. Results and discussion

The effects of operating pressure and corrugation angle on pressure drop and separation efficiency (HETP) of the B1 packing (surface area 250 m<sup>2</sup>/m<sup>3</sup>) are illustrated in Figs. 4 and 5, respectively. The pressure drop observed over the packed section of the column appears in Fig. 4. While there is little flow effect on the pressure drop in the preloading range, this is not the case as the loading region is approached. The loss in capacity with increasing operating pressure can be attributed to the increase in the liquid load. Clearly, the 60° packing has a capacity advantage over the 45° packing.

The efficiency curves shown in Fig. 5 give a clear indication of the effect of operating pressure on

throughput capacity. Efficiency improves with increasing operating pressure, but at the cost of decreased capacity. The deteriorating trend in efficiency with increasing  $F$ -factor is evident, and is similar but generally less pronounced with the expanded metal packings. The efficiency decreases up to the load point, beyond which efficiency first improves and then suddenly worsens coinciding with the flooding limit. At the highest oper-

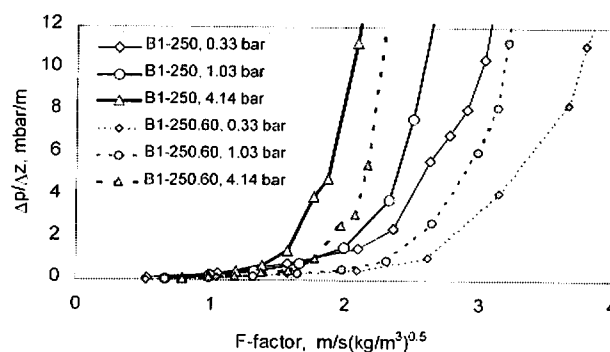


Fig. 4. Effect of operating pressure and corrugation angle on the hydraulic performance of similar size structured packings.

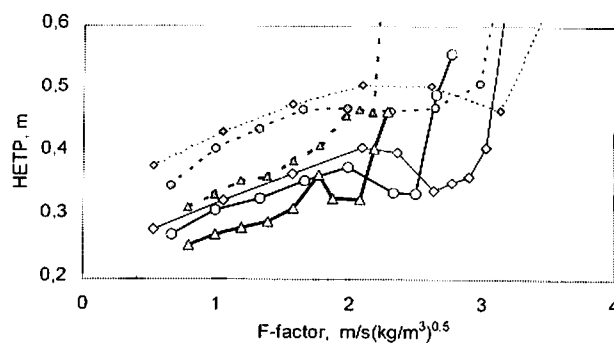


Fig. 5. Effect of operating pressure and corrugation angle on the mass transfer performance of similar size structured packings (the symbols are the same as in Fig. 4).

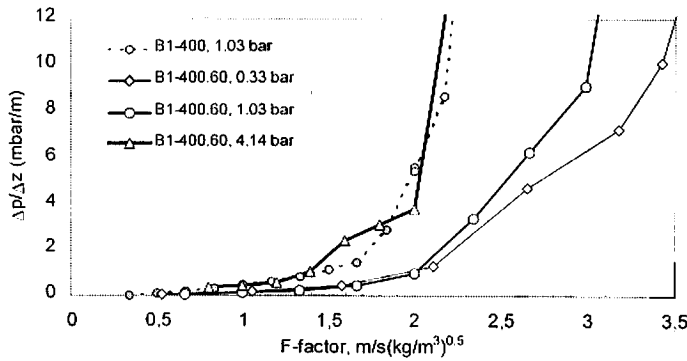


Fig. 6. Effect of corrugation angle on the hydraulic performance of structured packing with a larger surface area.

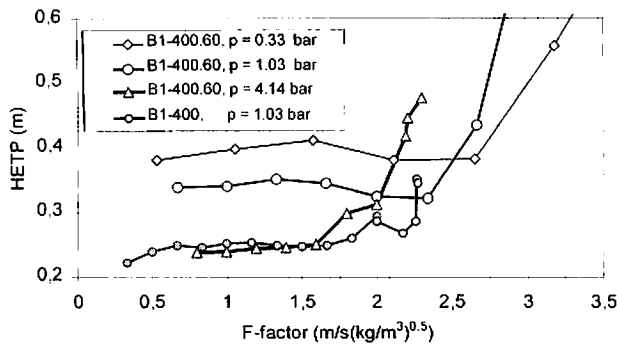


Fig. 7. Effect of corrugation angle on the mass transfer performance of structured packing with a larger surface area.

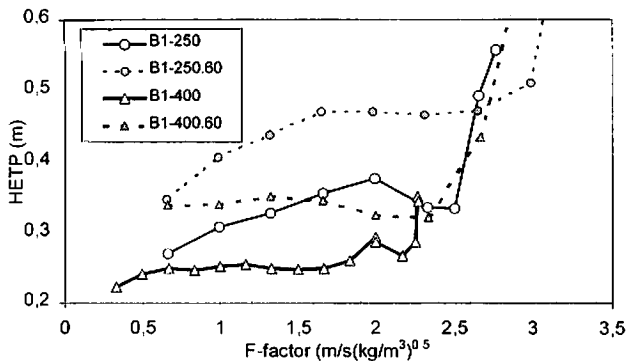


Fig. 8. Effect of specific surface area on the performance of the structured packing.

ating pressure there is a sudden loss of efficiency around the load point, which is similar to the so-called ‘efficiency hump’ observed with other packings at higher operating pressures [4,7]. As expected, beyond this point efficiency improves to some extent, which is not the case with the 60° packing. As illustrated in Figs. 6 and 7 similar operating pressure effects have been observed with larger surface area packings tested in this investigation.

The effect of the corrugation angle on mass transfer efficiency of a B1 packing (400 m<sup>2</sup>/m<sup>3</sup>) is shown in Fig. 8. The corresponding atmospheric pressure curves of

B1-250 are added to illustrate the effect of specific surface area. In general, the penalty for improved efficiency is obviously a decrease in capacity, and both characteristics are less pronounced than suggested by the ratio of the specific surface areas.

A much less pronounced effect of the *F*-factor on HETP is evident until the loading point is reached, beyond which a small hump-like disturbance in efficiency is noted. Again, this trend is not observed with the 60° packing. Similar to B1-250.60 at the highest operating pressure, the efficiency of B1-400.60 does not improve beyond the loading point. This probably results from a difference in the interaction between rising vapour and falling liquid at the transition between the packing layers when loading is reached [3]. Although the cross sectional area of the bottom and top of a gas flow channel is smaller in the 60° packing than in the 45° packing, the transition of both phases to an adjacent packing element is rather smooth. On the other hand, in the case of 45° packing, at loading point conditions, i.e. a relatively high liquid load, liquid from the element above drops off, forming a liquid-like curtain at the transition between the packing layers. This further reduces the available flow area for up-flowing vapour, which accelerates and entrains the droplets. As a result, additional contact area and efficiency results from the intense mixing at the transitions for the 45° packings. At very large liquid loads, such as encountered when operating at 4.14 bar, upon the onset of loading the liquid load causes the vapour to maldistribute, escaping to less loaded channels; this is generally accompanied by more backmixing in both phases.

The comparison of B1-400 and BSH-400 packings shown in Fig. 9 illustrates the effect of surface texturing or design. In the preloading range the HETP of the BSH packing is somewhat higher. While its installed surface is approximately 4% less than that of the B1 packing (see Table 1), 10% of the installed surface of the BSH is occupied by holes. The presence of these holes is probably the cause of the slightly larger capacity of the BSH packing. Without holes, the B1 packing

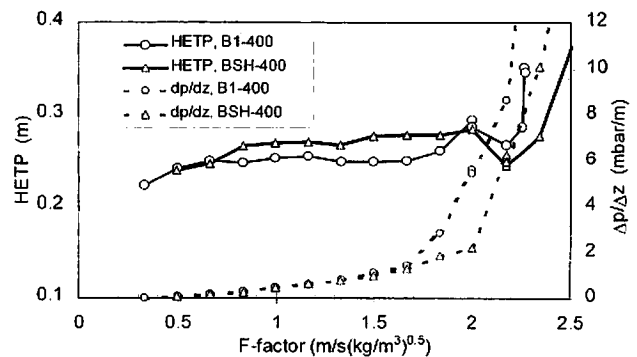


Fig. 9. Effect of the surface design on the performance of the structured packings.

Table 3  
Pressure drop and HETP at the loading point,  $p = 1.03$  bar

|                              | B1-250 | B1-250.60 | B1-400 | B1-400.60 | BSH-400 | BSH-400.60 |
|------------------------------|--------|-----------|--------|-----------|---------|------------|
| $F_{G,lp}$                   | 2      | 2.3       | 1.7    | 2         | 2       | 2.35       |
| $\Delta p/\Delta z$ (mbar/m) | 1.6    | 1         | 1.5    | 1         | 2.2     | 1.6        |
| HETP (m)                     | 0.38   | 0.47      | 0.25   | 0.32      | 0.28    | 0.37       |

Table 4  
Effects of the corrugation angle, specific surface area and surface design on pressure drop, capacity and efficiency of structured packings, expressed through ratios of compared design parameters<sup>a</sup>

|                     | B1-250    | B1-400    | BSH-400    | B1-400 (60) | B1-400  | B1-400.60  |
|---------------------|-----------|-----------|------------|-------------|---------|------------|
|                     | B1-250.60 | B1-400.60 | BSH-400.60 | B1-250 (60) | BSH-400 | BSH-400.60 |
| $\Delta p/\Delta p$ | 2.9       | 3         | 3          | 1.74 (1.8)  | 1.09    | 1.31       |
| $F_{G,lp}/F_{G,lp}$ | 0.86      | 0.84      | 0.85       | 0.81 (0.87) | 0.85    | 0.85       |
| HETP/HETP           | 0.79      | 0.71      | 0.73       | 0.71 (0.7)  | 0.93    | 0.83       |

<sup>a</sup> The values in brackets refer to the same size, 60° packing. The pressure drop and HETP ratios represent constant  $F$ -factor values.

forces the vapor to follow the channel whereas the perforated packings allow the vapour to flow at an effective angle that is slightly larger than the corrugation angle. At higher operating pressures the liquid loads are large enough to bridge common size holes (4 mm), thus forcing the gas to follow the channel as in the case of the B1 packing. The capacity of BSH is lower than that of B1 only at 4.14 bar.

For all packings at atmospheric pressure the measured values of the gas rate at loading, pressure drop and HETP at loading are shown in Table 3. It is clear that with increasing corrugation angle, the capacity increases with a corresponding decrease in efficiency. One should note that this is accompanied by a shift in the onset of loading to a lower pressure drop.

The relative performance of these packings is compared in Table 4, where ratios of pressure drops, loading point gas loads and HETP values of various packings at a constant  $F$ -factor are shown. In all cases an achieved gain in capacity with increased corrugation angle is penalised by a loss of efficiency. However, the differences in capacity and efficiency changes are an order of magnitude smaller than those in the measured pressure drops (roughly a factor of 3). The loss in efficiency is more pronounced in the case of the larger surface area packings. Also, the change in capacity and HETP caused by the difference in specific surface area is less than would be expected according to the ratio of the surface areas involved. On the other hand, the difference in pressure drop corresponds approximately with the ratio of the surface areas. The efficiency advantage of the B1 packing is a result of the 4% larger nominal surface area as well as the fact that the holes in the surface of the BSH occupy 10% of the nominal surface area. This is accompanied by a correspondingly

larger pressure drop. On the other hand, the presence of the holes contributes to a slightly larger capacity of BSH packings.

It should be noted that the trends in pressure drop and capacity are similar to those observed with the same packings in air–water hydraulic experiments. The air–water data have been useful in the development of the Delft model [8], which assumes various degrees of interaction between capacity and mass transfer efficiency on one hand and the three major components of pressure drop on the other. The effects of the corrugation angle on the relative magnitude of the three major pressure drop components is illustrated below, as predicted by the Delft method [8] for a total reflux distillation case (B1-250, cyclohexane– $n$ -heptane, 1.03 bar):

$$\Delta p/\Delta z = (\Delta p/\Delta z)_{GL} + (\Delta p/\Delta z)_{GG} + (\Delta p/\Delta z)_{DC}$$

|                         |      |      |      |
|-------------------------|------|------|------|
| 45°                     | 13%  | 43%  | 44%  |
| 60°                     | 24%  | 26%  | 50%  |
| $\zeta_{60}/\zeta_{45}$ | 0.81 | 0.27 | 0.52 |

Here, the subscripts GL, GG, and DC, stand for pressure losses related to the gas–liquid interaction, the gas–gas interaction at the crossings of the gas flow channels and the direction change at the transitions between packing elements. The symbol  $\zeta$  denotes overall gas–liquid friction factors.

For the case of packing with a corrugation angle of 45° the pressure drop due to the gas–liquid interaction, which is responsible for the intensity of mass transfer at the interface, represents only a minor percentage of the total pressure drop. Increasing the corrugation angle increases the relative contribution of the gas–liquid interaction as well as the direction change-imposed loss, both at the expense of dramatically reduced gas–gas

interaction. The last row in the above tabulation shows the absolute change in the components: the gas–liquid interaction change is only 20%, whereas the direction change losses are reduced by a factor of 2 and the gas–gas interaction losses by more than a factor of 3. This may explain the rather low loss of efficiency in this case, which indirectly indicates that only the pressure loss due to the gas–liquid interaction is fully involved with the mass transfer process. The gas–gas interaction is negligible, and the direction change losses corresponding to the enhancement due to entrance effects may play a role at lower gas loads when the gas flow is laminar. Therefore we may conclude that there is still a considerable potential for improvement of the performance of corrugated sheet structured packing, and this can be achieved if one finds a way to maximise ( $\Delta p_{\text{useful}}/\Delta p_{\text{useless}}$ ) appropriately.

#### 4. Conclusions

With increasing operating pressure, accompanied by an increased liquid load, the mass transfer performance of structured packings generally improves. However, this occurs at the expense of increased pressure drop and decreased capacity.

The mass transfer performance of a low specific surface packing deteriorates with increasing  $F$ -factor until the loading point is reached. This is more pronounced with the 45° packings than with the 60° packings. The performance of large specific surface packings is practically independent of the  $F$ -factor below the loading point. In general, the HETP curves of 45° B1 exhibit some sort of ‘efficiency hump’ around the loading point, which if eliminated, would improve the performance of a very good packing.

In all cases, except at the highest operating pressure, the mass transfer performance improves immediately above the loading point, and this trend is maintained until the onset of flooding. The loading region is generally broader for the 60° packing compared with the 45° packing.

With increasing corrugation angle, the pressure drop decreases sharply. The accompanying increase in capacity and decrease in mass transfer efficiency are an order of magnitude less pronounced, indicating that a significant amount of pressure drop is not directly involved with the mass transfer process. The loading point shifts generally to a higher  $F$ -factor for the 60° packing while the onset of loading occurs at a lower pressure drop.

The changes in pressure drop and HETP correspond approximately to changes in specific surface area. The capacity of the expanded metal packing is somewhat larger than that of the slightly more efficient closed surface packing (B1); this can be attributed to the holes in the surface.

A rather low percentage of total pressure drop is related to the mass transfer process, while more useful, i.e. the gas–liquid interaction pressure drop is encountered in the 60° packing. Increasing the ratio of ‘useful’ to ‘useless’ (the gas–gas interaction and direction change) pressure drop is the key to further improvement of the performance of corrugated sheet structured packings.

#### Acknowledgements

The authors wish to thank J. Montz GmbH for giving permission to publish these results, and are also grateful to J.A. Garcia and the SRP technical staff for their assistance with the measurements.

#### Appendix A. Nomenclature

|                      |  |
|----------------------|--|
| $A_p$                | specific packing surface area ( $\text{m}^2/\text{m}^3$ )  |
| $b_{\text{corr}}$    | corrugation base length (m)  |
| $F_G$                | gas load ( $F$ -factor) = $u_{G_s} \sqrt{\rho_G}$ (m/s ( $\text{kg}/\text{m}^3$ ) <sup>0.5</sup> ) |
| $F_{G,lp}$           | loading point gas load (m/s ( $\text{kg}/\text{m}^3$ ) <sup>0.5</sup> )                            |
| HETP                 | packing height equivalent to a theoretical plate (m)   |
| $h_{\text{corr}}$    | corrugation height (m)   |
| $h_{pe}$             | height of the packing element (m)  |
| $s_{\text{corr}}$    | corrugation side length (m)  |
| $u_{G_s}$            | superficial gas velocity (m/s)   |
| <i>Greek letters</i> |  |
| $\alpha$             | corrugation inclination angle (°)  |
| $\Delta p/\Delta z$  | pressure drop per unit bed height (mbar/m)   |
| $\varepsilon$        | packing void fraction (porosity) (–)   |
| $\rho_G$             | density of gas ( $\text{kg}/\text{m}^3$ )  |
| $\zeta$              | overall gas flow friction factor   |
| <i>Indices</i>       |  |
| DC                   | refers to gas flow direction change  |
| GG                   | refers to the gas–gas interaction  |
| GL                   | refers to the gas–liquid interaction   |
| 45                   | refers to the corrugation angle  |
| 60                   | refers to the corrugation angle  |

#### References

- [1] H. Kister, Distillation Design, McGraw-Hill, New York, 1992.
- [2] R. Billet, Packed Towers — In Process and Environmental Technology, VCH, Weinheim, 1995.

- [3] J.A. Rocha, J.L. Bravo, J.R. Fair, Distillation columns containing structured packings - a comprehensive model for their performance. 2. Mass transfer model, *Ind. Eng. Chem. Res.* 35 (1996) 1660–1667.
- [4] C.W. Fitz, J.G. Kunesh, A. Shariat, Performance of structured packing in a commercial scale column at pressures of 0.02 to 27.6 bar, *Ind. Eng. Chem. Res.* 38 (1999) 512–518.
- [5] Ž. Olujić, J. de Graauw, Effects of geometrical features on pressure drop of corrugated sheet structured packings, Paper No. 132f, AIChE Annual Meeting, San Francisco, 13–18 November 1994.
- [6] J.M. Lenoir, M. Sakata, The correlation of vapor–liquid equilibria used to determine tray efficiencies, *Ind. Eng. Chem. Fundam.* 17 (1978) 71–84.
- [7] F.J. Zuiderweg, Ž. Olujić, J.G. Kunesh, Liquid backmixing in structured packing in high pressure distillation, *ICHEME Symp. Ser.* 142 (1997) 865–872.
- [8] Ž. Olujić, Development of a complete simulation model for predicting the hydraulic and separation performance of distillation columns equipped with structured packings, *Chem. Biochem. Eng. Q.* 11 (1997) 31–46.